Segmentation of the Aorta Using Active Contours with Histogram-Based Descriptors

Miguel Alemán-Flores[1], Daniel Santana-Cedrés[1], Luis Alvarez[1], Agustín Trujillo[1], Luis Gómez[2], Pablo G. Tahoces[3], and José M. Carreira[4]

[1] CTIM, DIS, Universidad de Las Palmas de Gran Canaria, Spain
[2] CTIM, DIEA, Universidad de Las Palmas de Gran Canaria, Spain
[3] Dept Electronics and Computer Science, Universidad de Santiago, Spain
[4] Complejo Hospitalario Universitario de Santiago (CHUS), Spain
{miguel.aleman,lalvarez,agustin.trujillo,luis.gomez}@ulpgc.es
dsantana@ctim.es,{pablo.tahoces,josemartin.carreira}@usc.es

Abstract. This work presents an automatic method to segment the aortic lumen in computed tomography scans by combining an ellipse-based structure of the artery and an active contour model. The general shape of the aorta is first estimated by adapting the contour of its cross-sections to ellipses oriented in the direction orthogonal to the course of the vessel. From this set of ellipses, an initial segmentation is computed, which is used as starting approximation for the active contour technique. Apart from the traditional attraction and regularization terms of the active contours, an additional term is included to make the contour evolve according to the likelihood of a given intensity to be inside the aorta or in the surrounding tissues. With this technique, it is possible to adapt the boundary of the initial segmentation by considering not only the most significant edges, but also the distribution of the intensities inside and surrounding the aortic lumen.

Keywords: Aorta · Segmentation · Active Contours · CT.

1 Introduction

Computed tomography (CT) scans of the aorta provide the physicians with extremely valuable information for the diagnosis of several vascular pathologies, which include aneurysms, elongations, thrombi or dissections. A thorough analysis of the shape of the aorta is required to achieve a robust diagnosis. In this work, we present a method to obtain a segmentation of the aortic lumen by combining an initial approximation given by a series of ellipses which model the course of the aorta and a subsequent adjustment based on the active contour models. Furthermore, the latter is improved by extracting the intensity distributions inside the lumen and in the surrounding region to include statistical information in the evolution of the contour.

The extraction of the geometry of the aorta by means of a parameterized version of its cross-sections has been proposed in [3]. In [2], the contours of the

blood vessels are approximated by circles and these approximations are used to estimate the distribution of intensities in the inner and outer regions. On the other hand, the classical geodesic active contours, which allow adjusting an initial approximation of a contour to the most significant edges in the surrounding region, were introduced in [4]. A typical approach to implement these active contours consists in using level-set methods, which have also been applied to the segmentation of blood vessels [7]. In addition, some authors have previously presented the inclusion of statistical information in the level sets [5]. In [8], the boundary of the aorta is fitted using a cylindrical model. An overview of the different techniques for the segmentation of vessels in 3D image modalities can be found in [6]. In this work, we have combined the parameterized description of the contour of the artery with an extended version of the active contour model to extract a more precise segmentation of the aortic lumen in an automatic way.

2 Initial Approximation from Elliptical Cross-Sections

The shape of the aorta can be approximated by a curved tubular structure, in which three parts can be identified, namely the ascending aorta, the aortic arch and the descending aorta. In [3], the authors describe how this structure can be modeled using a collection of ellipses. In order to obtain a compact model of the vessel, the space between each consecutive pair of ellipses can be filled. Figure 1 illustrates the resulting ellipses using this algorithm and the volume generated from them. In [2], the authors obtain an estimation of the distribution of the intensities inside the aorta and in the surrounding tissues using a set of circles to sample the intensities inside and around the artery. Figure 2 illustrates the resulting probability density functions. Based on the results obtained in [3] and [2], we propose a new automatic segmentation technique which uses the set of ellipses to obtain an initial contour and the probability distribution to add a new term in the active contour formulation.

Fig. 1. Initial approximation: (left) set of ellipses obtained for the cross-sections of the aorta in the planes orthogonal to its flow, and (right) volume generated by filling the space between the ellipses.

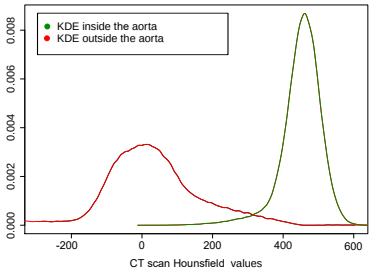

Fig. 2. Kernel density estimation of the intensities inside and around the aorta.

3 Adjustment of the Segmentation Using Active Contours

As mentioned above, we initially assumed that the cross-sections of the aorta can be modeled using ellipses. However, in some sections an ellipse cannot fit the contour in a completely satisfactory way. This usually happens due the presence of calcium deposits or mural thrombi, abrupt changes in the curvature of the aorta or even loss of the elliptic shape, mainly in the aortic root. For this reason, we propose to adapt the initial segmentation by means of the active contour technique. The classical formulation of this technique aims to adapt the contour in such a way that it moves locally toward the highest gradients, but preserving a certain degree of smoothness. Therefore, it usually consists of two terms which compete to reach a balance between contrast and regularity. The level set formulation of the geodesic active contours (GAC) described in [4] is given by

$$\frac{\partial u}{\partial t} = g_\sigma\left(I\right) \operatorname{div}\left(\frac{\nabla u}{\|\nabla u\|}\right)\|\nabla u\| + \nabla u \nabla g_\sigma\left(I\right), \tag{1}$$

where $\{(x, y, z) : u(t, x, y, z) < 0\}$ is an implicit representation of the volume to be optimized, I is the image on which the segmentation is performed and g_σ acts as a stop function. In our case, the initial approximation is given by the volume generated from the ellipses.

We must take into account that, in this work, the target organ is the aorta and, therefore, there is a range of intensities on which we must focus. Furthermore, some extreme intensities, such as those radiolucent regions corresponding to the lungs, could interfere in the evolution for the active contours, since they present clearly highlighted edges which could attract the contour toward false boundaries of the aorta. Consequently, we restrict the intensities to a given range of interest, in such a way that those intensities below the lower limit or above the upper limit are truncated to the lower or upper limit, respectively.

To determine these limits, we use the probability density functions estimated using the kernel density estimation described in [2]. This provides us with an estimation of the distribution inside the lumen $f_{in}(.)$ and in the surrounding tissues $f_{out}(.)$. Let P_{in}^n be the n^{th} percentile of the distribution $f_{in}(.)$ and let

P_{out}^m be the m^{th} percentile of the distribution $f_{out}(.)$, we can compute $\hat{I}$ as a truncated version of I as follows:

$$\hat{I}(x,y,z) = max\{P_{out}^m, \min\{P_{in}^n, I(x,y,z)\}\}, \tag{2}$$

where we assume that $P_{in}^n > P_{out}^m$. For the experiments we have selected P_{out}^{25} as the lower limit and P_{in}^{75} as the upper limit.

4 Active Contours with Histogram-Based Descriptors

The classical active contours provide a suitable technique to adapt a contour according to the magnitude of the gradient and the curvature of the contour. However, when extracting the contour of the aorta, we can also consider the fact that the intensities are distributed differently inside and outside the vessel. From the distributions $f_{in}(.)$ and $f_{out}(.)$ described in the previous section, we can build the following function:

$$k(I)(x,y,z) = \alpha \left(f_{out}(I(x,y,z)) - f_{in}(I(x,y,z)) \right), \tag{3}$$

where $\alpha \geq 0$, and $f_{in}(.)$, $f_{out}(.)$ provide us with the probability of a certain value to appear inside or outside the lumen. Therefore, the function k is positive if a given intensity I is more frequent in the outer region, and negative if it is more frequent inside the lumen. Moreover, the higher the disparity between both probabilities, the greater the magnitude of k, which means that the ambiguity is lower. This function can be used to guide the contour in such a way that it grows toward the surrounding regions which are more likely to be inside the lumen and shrinks where the voxels on the contour are more likely to belong to the outer region. This results in an expression as the following one:

$$\frac{\partial u}{\partial t} = g(\hat{I}_\sigma) div\left(\frac{\nabla u}{\|\nabla u\|}\right)\|\nabla u\| + \nabla g(\hat{I}_\sigma)\nabla u + k(I)\|\nabla u\|, \tag{4}$$

where $\hat{I}_\sigma$ is the smoothed version of the truncated image $\hat{I}$ using a Gaussian kernel of standard deviation σ. A mathematical study of this equation is presented in [1]. The stop function which has been used in the active contours is given by

$$g(\hat{I}_\sigma)(x,y,z) = \frac{1}{1+\lambda\|\nabla G_\sigma * \hat{I}(x,y,z)\|^2}, \tag{5}$$

where, in the experiments presented in this paper, $\lambda = 4/(P_{in}^{75} - P_{out}^{25})^2$ is introduced to adjust this function to the difference between the intensities of the inner and outer regions (indicated by the difference between the percentiles).

5 Results and Discussion

In order to test the accuracy of the proposed technique, we have selected 10 CT scans provided by the Department of Radiology of the University Hospital of

Santiago de Compostela (Spain), which have been segmented manually under the supervision of a radiologist. Some of these cases present severe pathologies, such as elongations, aneurysms, dissections or mural thrombi, including the presence of metal artifacts (like stents), which makes it really difficult to extract a precise segmentation. Figures 3(a)-(c) show how, in most cases, the active contours provide a better segmentation than the ellipses, and the introduction of the histogram-based term allows adjusting the contour in a more accurate way. The new proposal allows dealing with concavities and quite arbitrary shapes. Only in certain particular situations, the presence of lateral ramifications can make the active contour move away from the manual one (as shown in Fig. 3(d)).

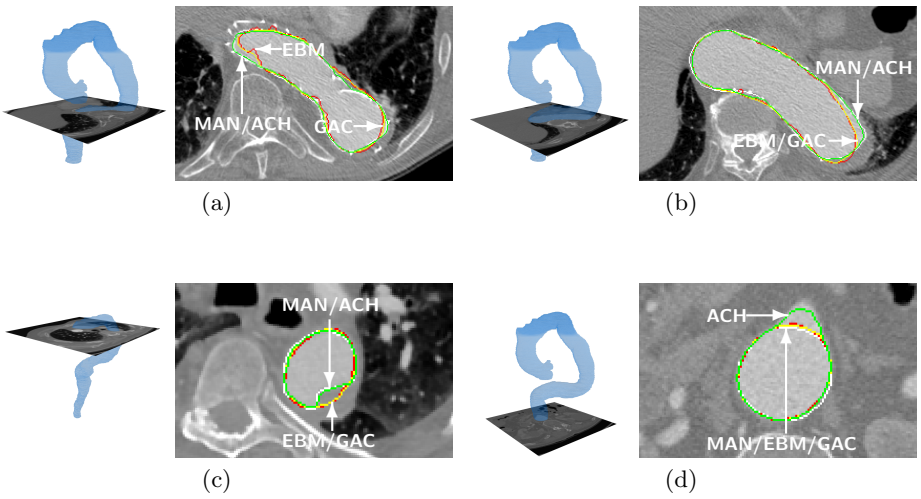

Fig. 3. Illustration of the performance of the segmentation techniques in 4 different slices (a)-(d). For each slice: (left) reference to the location of the cross-section in the course of the aorta, and (right) comparison of the manual segmentation (MAN/white) with the ellipse-based method (EBM/red), the geodesic active contours (GAC/yellow), and the active contours with histogram-based descriptors (ACH/green).

Three measures have been used to assess the accuracy of the results. First, the Dice similarity coefficient (DSC) measures how coincident the volumes covered by the manual segmentation S_m and the automatically extracted one S_a are:

$$DSC = \frac{2\,|S_m \cap S_a|}{|S_m| + |S_a|}. \tag{6}$$

Second, the bias estimator B_{pn} indicates whether the automatic segmentation S_a provides an over- (respectively under-) segmentation of S_m. It is given by:

$$B_{pn} = \frac{|S_a \backslash S_m| - |S_m \backslash S_a|}{|S_m \cap S_a|}, \tag{7}$$

where $|S_a \backslash S_m|$ and $|S_m \backslash S_a|$ compute the false positives and false negatives, respectively. Finally, the Euclidean distance from the voxels on the edge of the manual segmentation to those on the edge of the automatic one indicates how distant the contours are. Figures 4(a)-(c) show the closest point Euclidean distance from the manually delineated contour to those defined by the ellipses, the classical active contours and the active contours improved with the histogram-based term, respectively. As indicated by the colors, the number of voxels which are distant (in red) is reduced with respect to the ellipse-based volume when the active contours are applied, and even more if the histogram-based term is included. By considering the difference between the initial and final distances (Fig. 4(d)), we can see that the distance is similar or shorter in the vast majority of voxels, and some of them are significantly improved (bright green voxels).

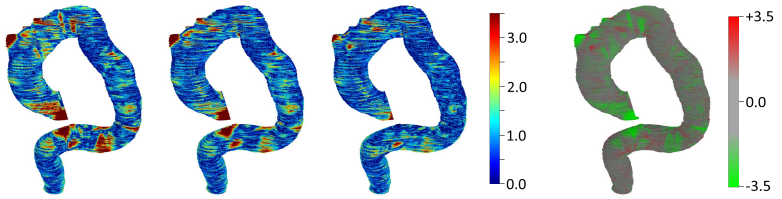

Fig. 4. Closest point Euclidean distance from the manual segmentation to the results provided by (a) the ellipses, (b) the geodesic active contours, and (c) the active contours with histogram-based descriptors (in mm), as well as (d) difference between (a) and (c) to illustrate the locations of the most significant changes.

Table 1 shows the average DSC and B_{pn}, as well as some statistics about the Euclidean distance, for the set of 10 CT scans. As observed, the mean DSC is increased by the active contours, and even more with the histogram-based term. On the other hand, the mean of the absolute B_{pn} is lower, which means that the bias has been reduced. Finally, the mean distance from the manual segmentation to the automatic one is significantly reduced, and so are the median and the 95^{th} percentile. The closest point Euclidean distance corresponding to these cases are shown in Fig. 5. Table 2 shows some statistics for each individual CT scan. As observed, the DSC is increased in all cases when the active contours are applied and, in all cases but one, it is even higher when the histogram-based term is included. Furthermore, the average Euclidean distance is reduced in all cases when the active contours are applied and, in all of them, the histogram-based term improves the results.

Table 1. Average results for the Dice similarity coefficient (DSC), the magnitude of the bias estimator B_{pn}, the mean distance, and different percentiles of the distance from the manual segmentation to the ellipse-based model (EBM), the adjustment with the geodesic active contours (GAC), and the improvement using the active contours with histogram-based descriptors (ACH) (in bold the best value for each measure).

	DSC	$\lvert B_{pn}\rvert$	$Distance$		
			$mean$	$P_{0.50}$	$P_{0.95}$
EBM	0.9458	0.0426	0.7946	0.7793	2.2235
GAC	0.9527	0.0373	0.7339	0.7555	2.0856
ACH	**0.9590**	**0.0159**	**0.5893**	**0.5830**	**1.5465**

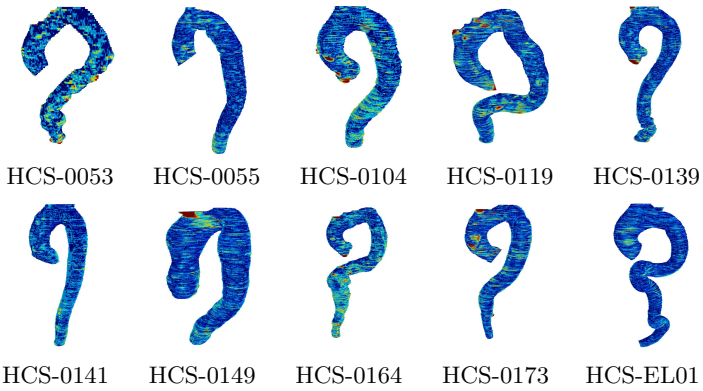

Fig. 5. Closest point Euclidean distance from the manual segmentation to that provided by the active contours with histogram-based descriptors in 10 different CT scans showing different pathologies.

Table 2. Dice similarity coefficient (DSC) and mean distance (in mm) obtained for 10 CT scans using the ellipse-based model (EBM), adjustment with the geodesic active contours (GAC), and improvement using the active contours with histogram-based descriptors (ACH) (in bold the best results for each case).

	DSC			$Mean\ Distance$		
Case	EBM	GAC	ACH	EBM	GAC	ACH
HCS-0053	0.9426	0.9477	**0.9549**	0.7595	0.7461	**0.5544**
HCS-0055	0.9423	0.9550	**0.9635**	0.7513	0.6412	**0.5207**
HCS-0104	0.9345	**0.9362**	0.9343	0.7915	0.7896	**0.7045**
HCS-0119	0.9492	0.9576	**0.9692**	1.0356	0.9089	**0.6365**
HCS-0139	0.9384	0.9538	**0.9623**	0.8780	0.7589	**0.5676**
HCS-0141	0.9411	0.9423	**0.9493**	0.6923	0.6901	**0.5678**
HCS-0149	0.9609	0.9677	**0.9712**	0.7611	0.6657	**0.5709**
HCS-0164	0.9333	0.9464	**0.9564**	0.9712	0.8478	**0.6613**
HCS-0173	0.9497	0.9520	**0.9588**	0.7639	0.7544	**0.6193**
HCS-EL01	0.9658	0.9680	**0.9700**	0.5412	0.5360	**0.4895**

6 Conclusion

The application of computer vision techniques to the analysis of medical images often requires extremely precise segmentations of certain organs or tissues. This is the case of the computer-aided diagnosis of several vascular pathologies. In this work, we have presented a new approach to the segmentation of the aorta, in which the extraction of its cross-sections by parameterizing them as ellipses is improved by means of the active contour technique. Furthermore, the addition of histogram-based descriptors to the classical formulation allows adjusting the shape of the contour in a more precise way. The results have demonstrated that the automatic segmentation which is obtained is closer to the manually delineated one. Not only has the DSC estimator been increased, but the Euclidean distance between the boundaries of both segmentations has been reduced. The good results for both measures support the idea that the combination of a parameterized description with the active contours, and the introduction of statistical information in the latter, can provide satisfactory segmentations of the aorta.

Acknowledgements. This research has partially been supported by the MINECO projects references TIN2016-76373-P (AEI/FEDER, UE) and MTM2016-75339-P (AEI/FEDER, UE) (Ministerio de Economía y Competitividad, Spain).

References

1. Alvarez, L., Cuenca, C., Díaz, J., González, E.: Level set regularization using geometric flows. SIAM Journal on Imaging Sciences **11**(2), 1493–1523 (2018)
2. Alvarez, L., González, E., Esclarín, J., Gomez, L., Alemán-Flores, M., Trujillo, A., Cuenca, C., Mazorra, L., Tahoces, P.G., Carreira, J.M.: Robust detection of circles in the vessel contours and application to local probability density estimation. In: MICCAI 2017 CVII-STENT, LNCS 10552. pp. 3–11. Springer (2017)
3. Alvarez, L., Trujillo, A., Cuenca, C., González, E., Esclarín, J., Gomez, L., Mazorra, L., Alemán-Flores, M., Tahoces, P.G., Carreira, J.M.: Tracking the aortic lumen geometry by optimizing the 3D orientation of its cross-sections. In: MICCAI 2017, LNCS 10434. pp. 174–181. Springer (2017)
4. Caselles, V., Kimmel, R., Sapiro, G.: Geodesic active contours. International Journal of Computer Vision **22**(1), 61–79 (1997)
5. Cremers, D., Rousson, M., Deriche, R.: A review of statistical approaches to level set segmentation: integrating color, texture, motion and shape. International Journal of Computer Vision **72**(2), 195–215 (2007)
6. Lesage, D., Angelini, E.D., Bloch, I., Funka-Lea, G.: A review of 3D vessel lumen segmentation techniques: Models, features and extraction schemes. Medical Image Analysis **13**(6), 819–845 (2009)
7. Manniesing, R., Niessen, W.: Local speed functions in level set based vessel segmentation. In: Barillot, C., et al. (eds.) Medical Image Computing and Computer-Assisted Intervention – MICCAI 2004. pp. 475–482. Springer (2004)
8. Xie, Y., Padgett, J., Biancardi, A.M., Reeves, A.P.: Automated aorta segmentation in low-dose chest CT images. International Journal of Computer Assisted Radiology and Surgery **9**(2), 211–219 (2014)